CuBTC Metal−Organic Framework Decorated with FeBTC Nanoparticles with Enhance Water Stability for Environmental Remediation Applications

Donghun Kim, Ik Ji Kim, Hyuk Taek Kwon, Keewook Paeng,* and Hoik Lee*
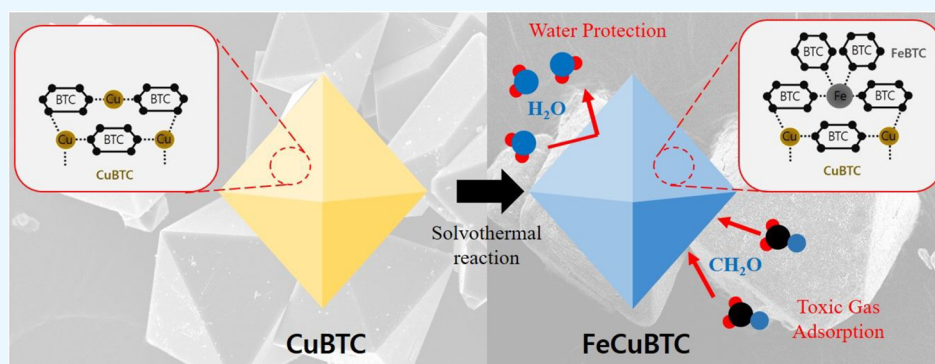
Read Online

ACCESS | Metrics & More | Article Recommendations | SI Supporting Information

ABSTRACT: Metal−organic frameworks (MOFs) based on Cu-benzene tricarboxylate (CuBTC) are widely used for gas storage and removal applications. However, they readily lose their crystal structures under humid conditions, limiting their practical applications. This structural decomposition reduces the specific surface area, gas adsorption capability, and recyclability of CuBTC considerably. In this study, a stable MOF against water exposure was designed based on FeBTC nanoparticle-covered CuBTC (FeCuBTC). A simple one-pot solvothermal process that enables the epitaxial growth of FeBTC on the CuBTC surface was proposed. Structural and morphological analyses after water exposure revealed that the water stability of FeCuBTC was better than that of CuBTC, which completely lost its crystallinity. This observed improvement in the water stability of the synthesized MOF proved to be beneficial for the adsorption of formaldehyde under humid conditions. The proposed strategy herein is simple yet highly effective in the design of hetero-bimetallic MOFs with considerably improved water resistance and extended applicability for environmental remediation processes.

1. INTRODUCTION

The presence of toxic pollutants in the atmosphere is becoming a global concern. Specifically, volatile organic compounds (VOCs), which are chemicals with vapor pressures greater than 10 Pa at 293 K as defined by the European Union, can cause photochemical smog and various diseases harmful to human health. The most common hazardous VOCs include formaldehyde, ammonia, and hydrosulfide.[1] Owing to the emissions from industrial chemical processes and building materials, VOCs are present in indoor and outdoor air.

Hybrid crystalline porous materials based on organic metal− ligands or metal−organic frameworks (MOFs) have been used for adsorption, catalysis, and sensing applications[2] owing to their unique properties, such as large surface area, tunable pore size, and unsaturated metal sites.[3] The structure of MOFs can be controlled effectively to achieve appropriate geometric size and specific chemical functionality by varying the types of organic ligands and metal ions.[4] As such, the chemical structure−property relationships of MOFs have been studied extensively to modify their target functionalities for their intended applications.[5]

Among the various MOFs, Cu-1, 3, 5-benzenetricarboxylate (CuBTC or HKUST-1) has high crystallinity and porosity, and excellent thermal stability.[6] Particularly, CuBTC exhibits a strong adsorption capacity for small molecules owing to its regular and small pore volume.[7] Moreover, CuBTC exhibits a highly active surface leading to its outstanding molecular adsorption capability. These properties render CuBTC suitable for environmental remediation applications. In addition, CuBTC has been regarded as a potential material for
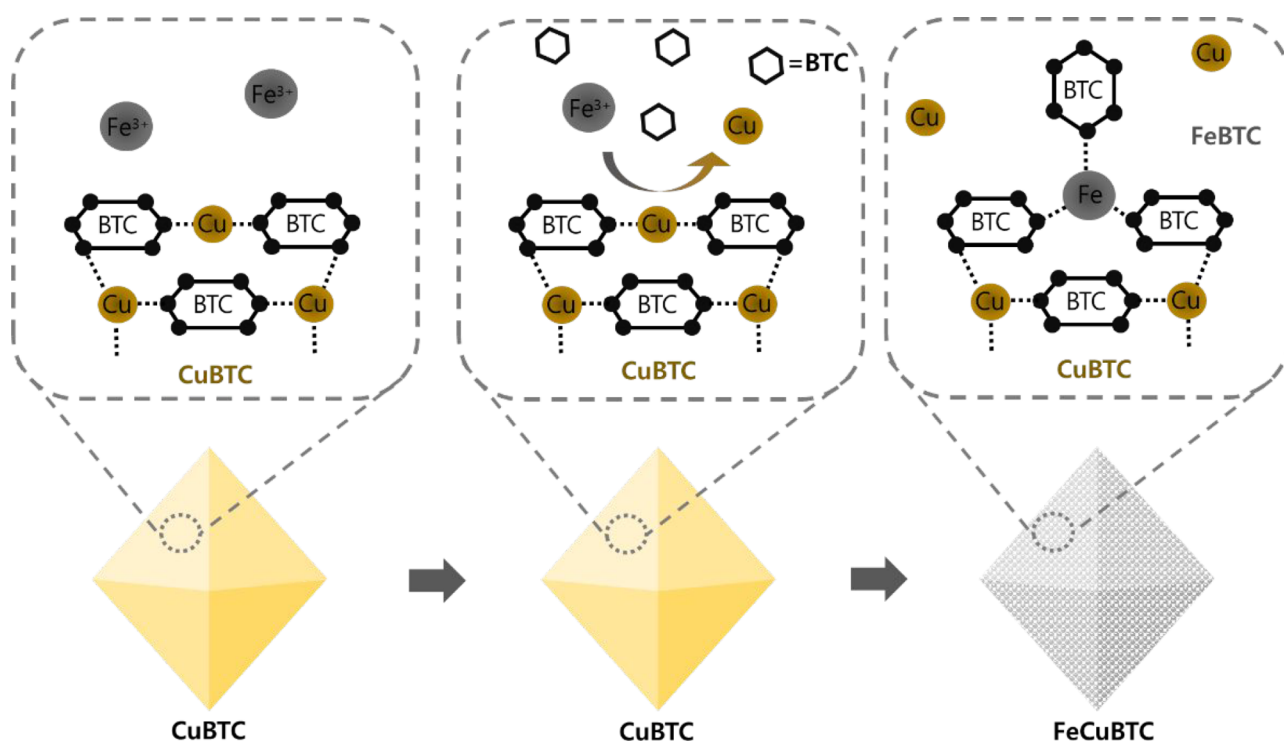
Figure 1. Formation mechanism of the FeBTC-layered CuBTC structure.

hydrocarbon separation,[8] gas storage including hydrogen,[9] and toxic gas removal.[10]

However, the poor water stability of CuBTC limits its applications despite its numerous desirable properties.[11] The active Cu(II) surface of CuBTC can interact with polar molecules, which makes it extremely sensitive to water and susceptible to irreversible degradation.[12] Ibarra and co-workers proposed a degradation mechanism to chemically rationalize the water instability of CuBTC through diffusion coefficient measurements and computational calculations.[13] Consequently, the stability of CuBTC should be improved to make it more suitable for practical applications.

The introduction of high-valence metal ions can improve the water stability of CuBTC.[14] The physicochemical properties of MOF can be tailored by doping metal ions into its framework. Sun and co-workers improved the porosity and stability of Zn-based MOF through a metal-ion metathesis process, which involved the replacement of Zn^{2+} ions with Cu^{2+} ions.[15] Lee and co-workers synthesized bimetallic Mn/Co MOFs as cathodes in Li−O$_2$ batteries.[16] The electrochemical stability of the Mn/Co MOF was better than that of the single metal MOF owing to the synergistic interaction between Mn and Co ions. In this study, an approach based on the introduction of a hetero-bimetallic framework is proposed to improve the water stability of CuBTC. The shell layer is composed of FeBTC, an analog of CuBTC, where Cu is replaced with Fe. The organic ligands in FeBTC can be shared with CuBTC. FeBTC is composed of Fe(II) units connected with BTC ligands. It has a pore dimension of 22 Å and a surface area of 1500 m^2/g.[17,18] FeBTC is widely used in catalytic,[19,20] membrane filtering,[21] water purification,[22] and gas adsorption applications.[23] Most importantly, it exhibits outstanding water stability.[24] The surface of CuBTC is coated with FeBTC (FeCuBTC) to prevent the decomposition of the CuBTC structure under humid conditions. The water uptake performance of

FeCuBTC was assessed to verify the improved stability of the bimetallic MOF against water. The enhanced stability further helps the adsorption of formaldehyde due to the water molecules in the FeCuBTC. Formaldehyde molecules interact effectively with water molecules by the formation of two hydrogen bonds through the water molecules.[25] Therefore, these results highlight that the novel core−shell type FeCuBTC structure can provide both improved water stability and adsorption capability of formaldehyde, possibly expanding the applicability of the FeCuBTC for gas-sensing material under humid conditions.

2. EXPERIMENTAL SECTION

2.1. Materials. CuBTC, FeBTC, iron(III) chloride hexahydrate (FeCl$_3$·6H$_2$O), and N,N-dimethylformamide (DMF, 99%) were purchased from Sigma-Aldrich (St. Louis, MO, USA) and were used without further purification.

2.2. Characterization. The morphology of the synthesized particles was examined using scanning electron microscopy (SEM; SU8010, HITACHI, Japan) and transmission electron microscopy (TEM; JEM-2100F, JEOL, Japan). The chemical compositions were analyzed using energy-dispersive X-ray spectroscopy (ThermoFisher, USA). Specimens for SEM were prepared by fixing the particle samples on carbon tape and coating them with Au (~15 nm) using an EMS 150 T ES turbomolecular pumped coating unit (Electron Microscopy Sciences, PA, USA) to impart sufficient conductivity to the samples. X-ray photoelectron spectroscopy (XPS; ESCA-LAB250, Thermo Scientific, UK) was employed to study the surface chemical compositions. C(1 s) peak at 284.6 eV was used as a reference for binding energy calibration. X-ray diffraction (XRD) patterns were recorded on a HyPix-400 (Rigaku, Japan) with Cu Kα radiation as the X-ray source, operating at 40 kV and 40 mA in the 2θ range of 5−45°. The specific surface area and pore size distribution were acquired

by interpreting the N_2 adsorption/desorption isotherms obtained at 77 K (ASAP 2010, Micromeritics, USA) using the Brunauer−Emmett−Teller (BET) and Barrett−Joyner−Halender (BJH) models. Prior to isotherm measurements, samples were degassed at 150 °C under the N_2 atmosphere overnight. The isotherm experiments were conducted in five replicates with a different sample for each sample. Water adsorption isotherms were collected at 35 °C by a constant volume adsorption apparatus (BELSORP-MAX II, BEL Japan). The water saturation pressure at 35 °C was approximately 0.0563 bar. Before the measurements, the samples were degassed at 100 °C for 12 h under vacuum. The gas adsorption of the MOFs was measured in a closed-loop system with a large gas-mixing chamber connected to a sample and a gas detector (1512i photoacoustic gas monitor, Luma Sense Technology) at room temperature. Formaldehyde (10 ppm) in the air was controlled by mixing formaldehyde gas and air using a gas controller. When the mixed gas in the gas chamber was equilibrated at the target concentration, it flowed through the sample, while the supply from outside was blocked to create a closed-loop circulation system. Thermogravimetric analysis (TGA Q500, TA Instruments, USA) was performed in the temperature range of 20−800 °C at a heating rate of 10 °C min^{-1} under the N_2 atmosphere.

2.3. Synthesis Process of FeCuBTC. CuBTC (0.65 g) and $FeCl_3\cdot6H_2O$ (0.19 g) were dissolved in DMF (3 mL). The resulting solution was sonicated for 10 min and then heated to 110 °C for 18 h, unless specified otherwise. The solution was phase-separated; the bottom, dark blue layer was subjected to centrifugation to collect the solid product. The resulting sample was dried at 175 °C for 5 h under a vacuum.

3. RESULTS AND DISCUSSION

The synthesis of the hetero-bimetallic FeCuBTC architecture, which was composed of FeBTC-coated CuBTC, involved the substitution reaction between the Cu^{2+} and Fe^{3+} ions and the epitaxial growth of the FeBTC MOF on the CuBTC surface during the solvothermal reaction at 110 °C. Figure 1 shows the decorating mechanism involving the substitution and epitaxial growth of the Fe^{3+} precursor. During the solvothermal reaction, the bond between the metal (Cu) and ligand (BTC) loosens, which allows the substitution of Cu with the Fe^{3+} ions in the precursor solution. Cu^{2+} ions can be substituted with Fe^{3+} owing to the difference in their reduction potentials. The lower reduction potential of the Fe^{3+} ions (−1.5 V) relative to that of Cu^{2+} (−1.2 V) induces the substitution reaction on the CuBTC surface.[26] Simultaneously, BTC molecules are released into the solution. Then, the coordinated Fe^{3+} ions in the CuBTC surface form new bonds with the free BTC molecules, consequently leading to the epitaxial growth of the FeBTC framework on the surface. When the surface is fully covered with FeBTC, a novel core−shell-like FeCuBTC structure, is attained.

The employed synthesis process in this study is described in detail in the Supporting Information. The morphology of the synthesized MOF was studied to confirm the formation of the hetero-bimetallic FeCuBTC, and optimize the synthetic process (Figures S1 and S2). After the optimization of synthesis parameters, FeCuBTC MOF was successfully synthesized. Figure 2a, b shows the SEM images of the FeBTC and CuBTC samples. On one hand, FeBTC was composed of aggregates of small, irregular particles with sizes ranging from 50 to 100 nm. On the other hand, CuBTC
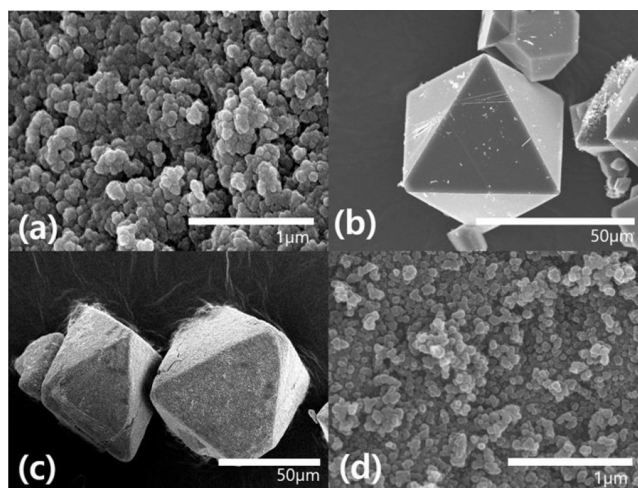

Figure 2. SEM images of (a) pristine FeBTC, (b) pristine CuBTC, (c) FeCuBTC synthesized after the solvothermal reaction, and (d) magnified image of the surface of the FeCuBTC particles.

exhibited a well-defined octahedral structure with a size ranging from 30 to 60 μm. The octahedral structure of CuBTC was maintained even after the solvothermal reaction performed to coat the original MOF with FeBTC (Figure 2c). However, the surface morphology of FeCuBTC was different from that of CuBTC. The surface of the CuBTC octahedrons was very smooth, and their vertices were sharp. In contrast, the surface of FeCuBTC was relatively rougher, and its vertices were blunt. Interestingly, the surface of FeCuBTC (Figure 2d) was covered with small, irregular particle aggregates, which are very similar to those on the FeBTC surface (Figure 2a). These observations strongly suggest that the FeCuBTC surface is covered by FeBTC, demonstrating a core−shell-like structure. The surfaces of the particles were further examined through TEM (Figure S3). The FeCuBTC surface was less dense than that of the pristine CuBTC. Furthermore, its morphology was similar to that of FeBTC. The thickness of the shell layer measured from the TEM image was approximately 0.4 μm.

The internal structure of FeCuBTC was comparable to that of CuBTC. The elemental mapping images of FeCuBTC (Figure S4) confirmed the presence of Fe and Cu in the hetero-bimetallic MOF. (Atomic ratio of Cu:Fe = 10.1:2.9) Overall, these results confirm the successful growth and demonstrate the uniform distribution of FeBTC over the CuBTC surface, thereby forming the FeCuBTC structure. To further characterize the hetero-bimetallic MOF, XPS was also performed. The peak positions corresponding to Cu, Fe, C, and O in the full XPS spectrum of FeCuBTC are similar to those in the full spectra of CuBTC and FeBTC (Figures S5 and S6). The multiplex Cu 2p spectra of FeCuBTC and CuBTC can be deconvoluted into Cu 2p3/2 and Cu 2p1/2 regions. The binding energies of the Cu species in FeCuBTC and CuBTC were similar. The Fe 2p spectra of FeCuBTC can be divided into Fe 2p3/2 and Fe 2p1/2 regions. Interestingly, the Fe 2p peaks of FeCuBTC corresponded well with those of FeBTC, thereby confirming the successful formation of FeBTC on CuBTC.

To study the crystal structures of the hetero-bimetallic FeCuBTC, and pristine FeBTC and CuBTC MOFs, XRD was performed (Figure S7). Pristine FeBTC and CuBTC exhibited typical XRD patterns with characteristic diffraction peaks consistent with those in previous reports.[27] A series of weak

peaks superimposed on the pattern background, which is characteristic of materials with low degrees of crystallinity, was observed in the XRD pattern of FeBTC. In contrast, the XRD pattern of CuBTC featured strong diffraction peaks at $2\theta = 6.8$, 9.6, 11.7, 13.5, 14.7, 15.1, 17.6, 20.3, 26.0, and 29.4°, which can be indexed to the face-centered cubic facets (200), (220), (222), (400), (331), (420), (511), (440), (553), and (555), respectively.[28] Similar characteristic peaks were observed in the diffraction pattern of FeCuBTC (Figure S7c), indicating that the high degree of crystallinity of FeCuBTC originated from CuBTC. The diffraction pattern of CuBTC was almost preserved, which implies that the crystal structure of the CuBTC core was not damaged during the solvothermal reaction. The characteristic peak at 10.9° in the XRD pattern of FeBTC was barely observed in that of FeCuBTC. The differences between the diffraction patterns of FeBTC and FeCuBTC were observed at $2\theta = 9-13°$. The peak at 10.9° was assumed to emerge as a shoulder of the peak at 11.7°. Most of the XRD peaks of FeBTC were possibly masked by the well-defined peaks of the crystalline CuBTC MOF; the peak at 10.9° corresponding to FeBTC was only observed as a shoulder.

The specific surface area and pore size distribution of the hetero-bimetallic FeCuBTC MOF were characterized through the BET and BJH models using the N_2 gas adsorption/desorption isotherms (Figure S8). The estimated specific surface areas of CuBTC and FeBTC were 1433.31 ± 26.23 and 982.18 ± 33.81 m^2/g, respectively. The specific surface area of FeCuBTC was 1586.98 ± 38.47 m^2/g, which was approximately 11% higher than that of CuBTC. The observed increase in the specific surface area can be attributed to the growth of FeBTC on the CuBTC surface. It is assumed that the generation of FeBTC nanoparticles has happened largely than the amount of Cu ions substitution, and the formation of FeBTC on CuBTC creates the additional porous structure, thereby increasing the specific surface area of the MOF. A similar phenomenon was also observed in MIL-101 (Cr, Mg), Ni-doped MOF-5, alkali metal cation doped MOF-5, and Fe-doped CuBTC, supporting the BET results of FeCuBTC.[29-33] Type IV N_2 adsorption isotherms were recorded, implying that the samples had mesoporous structures. The average pore diameter of FeCuBTC was 2.1 nm, which is comparable to those of CuBTC (1.9 nm) and FeBTC (2.0 nm). At small Fe dopant concentrations, Fe blocks the pores of the CuBTC MOF structure, thereby reducing the specific surface area and pore volume.[34] However, the core−shell structure of the synthesized FeCuBTC in this study was beneficial for maintaining the structure of both MOF phases. As such, the pore-blocking tendency of the Fe dopants was not observed, which demonstrates an advantage of a hetero-bimetallic MOF structure.

To determine the water resistance of the synthesized MOFs, their H$_2$O uptake behaviors were evaluated. Figure S9 shows the volume of the adsorbed water per unit weight of the MOFs as a function of relative humidity (RH). At 100% RH, FeBTC exhibited a relatively low water adsorption capability (148.2 cm^3/g). In contrast, under the same conditions, the water adsorption capacity of CuBTC was higher at 573.7 cm^3/g, which is approximately 3.5 times higher than that of FeBTC. The adsorption capability of FeCuBTC at 100% RH was 506.5 cm^3/g, which is comparable but slightly lower than that of CuBTC. Considerable differences were observed at 62% RH:

262.07 cm^3/g for CuBTC, 106.6, and 405.2 cm^3/g for FeCuBTC.

At this condition, FeCuBTC exhibited moderate water adsorption capacity, suggesting that the FeBTC shell layer affected the water uptake. The average annual humidity in Seoul, Korea, and New York, USA are 62 and 63%, respectively (data obtained from the Korea Meteorological Administration and U.S. National Weather Service). Considering this, FeCuBTC can be used for practical applications. Water molecules can easily bind to the available sites of CuBTC and subsequently attack the Cu−O coordination bond, displacing the ligands through hydrolysis and resulting in the structural collapse of the MOF.[35,36] Misra co-workers reported that structural collapse after the exposure of CuBTC to water for 2 h resulted in a 93.3 and 93.5% reduction in the specific surface area and pore volume, respectively.[14] Fan et al. also reported the irreversible degradation of CuBTC at 90% RH, which led to a reduction in the adsorption capacity. The achieved reduction in the water uptake capacity of the hetero-bimetallic MOF indicates its improved water resistance. Therefore, the structural collapse due to the interaction with water molecules was inhibited effectively.

The structural stability of the synthesized MOFS underwater exposure was further investigated through SEM, XRD, and BET. Figure 3a shows the SEM image of CuBTC after
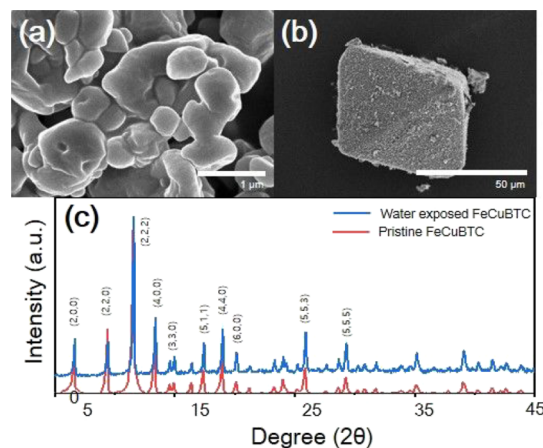

Figure 3. SEM images of (a) CuBTC and (b) FeCuBTC samples and (c) their X-ray diffraction (XRD) patterns after immersion in water for 24 h.

immersion in water for 24 h. The original morphology was completely lost. A random sphere-like morphology was observed instead of an octahedral structure. In contrast, the octahedral structure of FeCuBTC was fully preserved even after its exposure to water for 24 h (Figure 3b). These results further demonstrate the improved water stability of FeCuBTC owing to the low water affinity of its FeBTC shell. The XRD profile of FeCuBTC upon exposure to water (Figure 3c) was almost similar to that of pristine FeCuBTC, implying that these samples had the same crystal structure. Moreover, the water did not degrade the original crystal structure of the hetero-bimetallic MOF. Furthermore, the N_2 adsorption/desorption isotherms of FeCuBTC did not change significantly after water exposure (Figure S10), which corresponds to the SEM and XRD results. The N_2 adsorption/desorption isotherms of FeCuBTC also show the same type IV as before exposure to water.

The water uptake behavior without structural collapse can be favorable for formaldehyde adsorption. Typically, MOFs can adsorb small molecules by trapping them inside the nanopores, facilitating the adsorption of specific molecules.[37,38] However, as previously discussed, water molecules can cause a complete structural collapse for some MOFs, deteriorating their adsorption capability.[11] The MOF structure without moisture-induced structural collapse leads to a synergistic effect due to the interaction of toxic gas molecules with water. Humphrey and co-workers synthesized a specific MOF (Mg-CUK-1) that did not collapse even after several water adsorption/desorption cycles.[39] The hetero-bimetallic Fe-CuBTC MOF produced in this study also exhibited considerable toxic gas adsorption capacity under humid conditions without structural collapse.

For formaldehyde adsorption, most adsorbents are typically designed to incorporate amine or hydroxy groups to induce hydrogen bonds to the formaldehyde. Shen and co-workers introduced *o*-phenylenediamine (OPD) into CuBTC nanopore structure to detect formaldehyde. They exploited the strong affinity between CuBTC and OPD toward an effective sensing system for gaseous formaldehyde.[40] Kim and co-workers tailored a MOF structure (UiO-66) to incorporate amine functionality that exhibits a strong affinity for formaldehyde.[41] The presence of the NH_2 group in the MOF structure played a key role in capturing formaldehyde. These results support that the functional group is necessary for the adsorbent to interact with formaldehyde.

Figure 4 shows the formaldehyde adsorption behavior of the synthesized MOFs. The total formaldehyde gas uptake
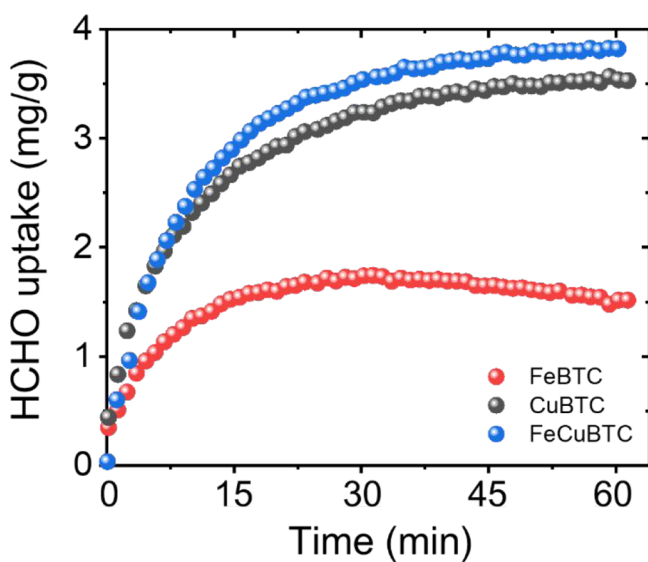

Figure 4. Formaldehyde gas uptake capacity of CuBTC, FeBTC, and FeCuBTC from 0 to 60 min. The uptake capacity of each MOF was measured after a water vapor adsorption test.

capacities of CuBTC, FeBTC, and FeCuBTC were 3.6, 2.1, and 3.8 mg/g, respectively. It is worth noting that the adsorption capacity value of the FeCuBTC is higher than pitch-based activated carbon fiber (ACF) (almost eight times),[37] indicating that the FeCuBTC also can be used for toxic gas adsorption material instead of the ACF. Notably, the adsorption capacity of FeBTC was the lowest; CuBTC and FeCuBTC exhibited much higher adsorption capacities

because of their capability to trap water molecules in their nanopores. Formaldehyde exhibits a high affinity toward water molecules, which makes the higher gas adsorption performance of CuBTC and FeCuBTC feasible.[25] On one hand, the better formaldehyde adsorption capability of CuBTC than that of FeBTC originated from water molecules. Structural collapse was observed for the CuBTC MOF after water exposure. As such, the enhanced toxic gas adsorption properties of CuBTC cannot be attributed to its structure and properties. In summary, FeCuBTC exhibited considerable adsorption capacity and retained its crystal structure under humid conditions, opening the possibility of enhancing the hydro-stability of the MOF and improving its applicability for environmental remediation applications. In particular, since most sensors are highly sensitive to moisture, these results highlight the applicability of FeCuBTC for gas-sensing materials under humid conditions.

4. CONCLUSIONS

In summary, the novel FeCuBTC core−shell type structure produced in this study demonstrated better hydrolytic stability and greater toxic gas adsorption capacity than the CuBTC precursor under humid conditions. A one-pot solvothermal method was employed to coat CuBTC with FeBTC. The crystalline structure of the CuBTC core was fully preserved after the solvothermal reaction. The successful synthesis of FeBTC-layered CuBTC structure with a large specific surface area was confirmed through different characterization methods. More importantly, unlike the CuBTC precursor, the hetero-bimetallic FeCuBTC MOF maintained its original crystallinity even after exposure to water. Therefore, the introduction of the FeBTC shell rendered excellent water resistance and improved the hydrolytic stability of the MOFs, which prevented the structural collapse of FeCuBTC in the presence of water. Furthermore, the adsorbed water molecules in the nanopores of the MOFs were beneficial in the formaldehyde gas adsorption under humid conditions. Therefore, the core−shell type MOF structure is an attractive design to improve the hydrostability and consequently, to expand its applicability for environmental protection and remediation, such as toxic gas removal and sensing.

■ ASSOCIATED CONTENT

ⓈI Supporting Information

The Supporting Information is available free of charge at https://pubs.acs.org/doi/10.1021/acsomega.2c05338.

> Preparation of FeCuBTC, details of material characterization, TEM images of pristine FeBTC, pristine CuBTC and FeCuBTC, SEM-EDS image of FeCuBTC, XRD patterns of pristine FeBTC, pristine CuBTC, and FeCuBTC, N_2 adsorption/desorption isotherms, and H_2O vapor adsorption isotherm (PDF)

■ AUTHOR INFORMATION

Corresponding Authors

Keewook Paeng − *Department of Chemistry, Sungkyunkwan University, Suwon, Gyeonggi-do 16419, Republic of Korea;* ⓞ orcid.org/0000-0001-5837-621X; Email: paeng@skku.edu

Hoik Lee − *Advanced Textile R&D Department, Korea Institute of Industrial Technology (KITECH), Ansan-si,*

Gyeonggi-do 15588, Republic of Korea; ⊙ orcid.org/0000-0002-9412-2273; Email: hoik@kitech.re.kr

Authors

Donghun Kim − *Advanced Textile R&D Department, Korea Institute of Industrial Technology (KITECH), Ansan-si, Gyeonggi-do 15588, Republic of Korea; Department of Chemistry, Sungkyunkwan University, Suwon, Gyeonggi-do 16419, Republic of Korea;* ⊙ orcid.org/0000-0003-4221-3680

Ik Ji Kim − *Department of Chemical Engineering, Pukyong National University, Busan 48513, Republic of Korea*

Hyuk Taek Kwon − *Department of Chemical Engineering, Pukyong National University, Busan 48513, Republic of Korea*

Complete contact information is available at:
https://pubs.acs.org/10.1021/acsomega.2c05338

Notes

The authors declare no competing financial interest.

■ REFERENCES

(1) Barea, E.; Montoro, C.; Navarro, J. A. R. Toxic gas removal − metal−organic frameworks for the capture and degradation of toxic gases and vapours. *Chem. Soc. Rev.* **2014**, *43*, 5419−5430.

(2) Zhou, H.-C. J.; Kitagawa, S. Metal−Organic Frameworks (MOFs). *Chem. Soc. Rev.* **2014**, *43*, 5415−5418.

(3) Uemura, T.; Yanai, N.; Kitagawa, S. Polymerization reac-tions in porous coordination polymers. *Chem. Soc. Rev.* **2009**, *38*, 1228−1236.

(4) Yao, Y.; Wang, C.; Na, J.; Hossain, M. S. A.; Yan, X.; Zhang, H.; Amin, M. A.; Qi, J.; Yamauchi, Y.; Li, J. Macroscopic MOF Architectures: Effective Strategies for Practical Application in Water Treatment. *Small* **2022**, *18*, No. 2104387.

(5) Meng, J.; Liu, X.; Niu, C.; Pang, Q.; Li, J.; Liu, F.; Liu, Z.; Mai, L. Advances in metal−organic framework coatings: versatile synthesis and broad applications. *Chem. Soc. Rev.* **2020**, *49*, 3142−3186.

(6) Gascon, J.; Aguado, S.; Kapteijn, F. Manufacture of dense coatings of Cu3(BTC)2 (HKUST-1) on α-alumina. *Microporous Mesoporous Mater.* **2008**, *113*, 132−138.

(7) Dai, Y.; Li, M.; Liu, F.; Xue, M.; Wang, Y.; Zhao, C. Graphene oxide wrapped copper-benzene-1,3,5-tricarboxylate metal organic framework as efficient absorbent for gaseous toluene under ambient conditions. *Environ. Sci. Pollut. Res.* **2019**, *26*, 2477−2491.

(8) Wu, Y.; Sun, Y.; Xiao, J.; Wang, X.; Li, Z. Glycine-Modified HKUST-1 with Simultaneously Enhanced Moisture Stability and Improved Adsorption for Light Hydrocarbons Separation. *ACS Sustainable Chem. Eng.* **2019**, *7*, 1557−1563.

(9) Lin, K.-S.; Adhikari, A. K.; Ku, C.-N.; Chiang, C.-L.; Kuo, H. Synthesis and characterization of porous HKUST-1 metal organic frameworks for hydrogen storage. *Int. J. Hydrogen Energy* **2012**, *37*, 13865−13871.

(10) Borfecchia, E.; Maurelli, S.; Gianolio, D.; Groppo, E.; Chiesa, M.; Bonino, F.; Lamberti, C. Insights into Adsorption of NH3 on HKUST-1 Metal−Organic Framework: A Multitechnique Approach. *J. Phys. Chem. C* **2012**, *116*, 19839−19850.

(11) Dahanayaka, M.; Babicheva, R.; Chen, Z.; Law, A. W.-K.; Wu, M. S.; Zhou, K. Atomistic simulation study of GO/HKUST-1 MOF

membranes for seawater desalination via pervaporation. *Appl. Surf. Sci.* **2020**, *503*, No. 144198.

(12) Al-Janabi, N.; Hill, P.; Torrente-Murciano, L.; Garforth, A.; Gorgojo, P.; Siperstein, F.; Fan, X. Mapping the Cu-BTC metal−organic framework (HKUST-1) stability envelope in the presence of water vapour for CO2 adsorption from flue gases. *Chem. Eng. J.* **2015**, *281*, 669−677.

(13) Álvarez, J. R.; Sánchez-González, E.; Pérez, E.; Schneider-Revueltas, E.; Martínez, A.; Tejeda-Cruz, A.; Islas-Jácome, A.; González-Zamora, E.; Ibarra, I. A. Structure stability of HKUST-1 towards water and ethanol and their effect on its CO 2 capture properties. *Dalton Trans.* **2017**, *46*, 9192−9200.

(14) Goyal, P.; Paruthi, A.; Menon, D.; Behara, R.; Jaiswal, A.; Kumar, A.; Krishnan, V.; Misra, S. K. Fe doped bimetallic HKUST-1 MOF with enhanced water stability for trapping Pb(II) with high adsorption capacity. *Chem. Eng. J.* **2022**, *430*, No. 133088.

(15) Yang, J.; Wang, X.; Dai, F.; Zhang, L.; Wang, R.; Sun, D. Improving the Porosity and Catalytic Capacity of a Zinc Paddlewheel Metal-Organic Framework (MOF) through Metal-Ion Metathesis in a Single-Crystal-to-Single-Crystal Fashion. *Inorg. Chem.* **2014**, *53*, 10649−10653.

(16) Kim, S. H.; Lee, Y. J.; Kim, D. H.; Lee, Y. J. Bimetallic Metal−Organic Frameworks as Efficient Cathode Catalysts for Li−O2 Batteries. *ACS Appl. Mater. Interfaces* **2018**, *10*, 660−667.

(17) Sciortino, L.; Alessi, A.; Messina, F.; Buscarino, G.; Gelardi, F. M. Structure of the FeBTC Metal−Organic Framework: A Model Based on the Local Environment Study. *J. Phys. Chem. C* **2015**, *119*, 7826−7830.

(18) Opanasenko, M.; Dhakshinamoorthy, A.; Shamzhy, M.; Nachtigall, P.; Horáček, M.; Garcia, H.; Čejka, J. Comparison of the catalytic activity of MOFs and zeolites in Knoevenagel condensation. *Catal. Sci. Technol.* **2013**, *3*, 500−507.

(19) Vu, H. T.; Nguyen, M. B.; Vu, T. M.; Le, G. H.; Pham, T. T. T.; Nguyen, T. D.; Vu, T. A. Synthesis and Application of Novel Nano Fe-BTC/GO Composites as Highly Efficient Photocatalysts in the Dye Degradation. *Top. Catal.* **2020**, *63*, 1046−1055.

(20) Martínez, F.; Leo, P.; Orcajo, G.; Díaz-García, M.; Sanchez-Sanchez, M.; Calleja, G. Sustainable Fe-BTC catalyst for efficient removal of mehylene blue by advanced fenton oxidation. *Catal. Today* **2018**, *313*, 6−11.

(21) Kim, D.; Kim, Y.; Kim, D.; Son, D.; Doh, S. J.; Kim, M.; Lee, H.; Yoon, K. R. Rational Process Design for Facile Fabrication of Dual Functional Hybrid Membrane of MOF and Electrospun Nanofiber towards High Removal Efficiency of PM2.5 and Toxic Gases. *Macromol. Rapid Commun.* **2022**, *43*, No. 2100648.

(22) Liu, H.; Jiang, C.; Li, H.; Chen, Z. Preparation of FeBTC/silica aerogels by a co-sol-gel process for organic pollutant adsorption. *Mater. Res. Express* **2019**, *6*, 1250g7.

(23) Zukal, A.; Opanasenko, M.; Rubeš, M.; Nachtigall, P.; Jagiello, J. Adsorption of pentane isomers on metal-organic frameworks Cu-BTC and Fe-BTC. *Catal. Today* **2015**, *243*, 69−75.

(24) Burtch, N. C.; Jasuja, H.; Walton, K. S. Water Stability and Adsorption in Metal−Organic Frameworks. *Chem. Rev.* **2014**, *114*, 10575−10612.

(25) Liu, C.; Yan, S.; Chen, D. The adsorption mechanism of formaldehyde molecules on ZnO-SAW sensor at a different relative humidity. *Results Phys.* **2021**, *26*, No. 104442.

(26) Nageswaran, G. Review—Direct Electrochemical Synthesis of Metal Organic Frameworks. *J. Electrochem. Soc.* **2020**, *167*, 155527.

(27) Lara-Serrano, M.; Morales-delaRosa, S.; Campos-Martin, J. M.; Abdelkader-Fernández, V. K.; Cunha-Silva, L.; Balula, S. S. Isomer-ization of glucose to fructose catalyzed by metal−organic frameworks. *Sustain. Energy Fuels* **2021**, *5*, 3847−3857.

(28) Chen, Y.; Mu, X.; Lester, E.; Wu, T. High efficiency synthesis of HKUST-1 under mild conditions with high BET surface area and CO2 uptake capacity. *Prog. Nat. Sci.* **2018**, *28*, 584−589.

(29) Sun, X.; Gu, X.; Xu, W.; Chen, W.-J.; Xia, Q.; Pan, X.; Zhao, X.; Li, Y.; Wu, Q.-H. Novel Hierarchical Fe(III)-Doped Cu-MOFs With Enhanced Adsorption of Benzene Vapor. *Front. Chem.* **2019**, *7*, 652.

(30) Zhou, Z.; Mei, L.; Ma, C.; Xu, F.; Xiao, J.; Xia, Q.; Li, Z. A novel bimetallic MIL-101(Cr, Mg) with high CO_2 adsorption capacity and CO_2/N_2 selectivity. *Chem. Eng. Sci.* **2016**, *147*, 109−117.

(31) Li, H.; Shi, W.; Zhao, K.; Li, H.; Bing, Y.; Cheng, P. Enhanced Hydrostability in Ni-Doped MOF-5. *Inorg. Chem.* **2012**, *51*, 9200−9207.

(32) Chu, C. L.; Chen, J. R.; Lee, T. Y. Enhancement of hydrogen adsorption by alkali-metal cation doping of metal-organic framework-5. *Int. J. Hydrogen Energy* **2012**, *37*, 6721−6726.

(33) Song, L.; Xue, C.; Xia, H.; Qiu, S.; Sun, L.; Chen, H. Effects of Alkali Metal (Li, Na, and K) Incorporation in NH_2−MIL125(Ti) on the Performance of CO_2 Adsorption. *Materials* **2019**, *12*, 844.

(34) Ambroz, F.; Macdonald, T. J.; Martis, V.; Parkin, I. P. Evaluation of the BET Theory for the Characterization of Meso and Microporous MOFs. *Small Methods* **2018**, *2*, No. 1800173.

(35) Zou, M.; Dong, M.; Zhao, T. Advances in Metal-Organic Frameworks MIL-101(Cr). *Int. J. Mol. Sci.* **2022**, *23*, 9396.

(36) Low, J. J.; Benin, A. I.; Jakubczak, P.; Abrahamian, J. F.; Faheem, S. A.; Willis, R. R. Virtual high throughput screening confirmed experimentally: porous coordination polymer hydration. *J. Am. Chem. Soc.* **2009**, *131*, 15834−15842.

(37) Song, Y.; Qiao, W.; Yoon, S.-H.; Mochida, I.; Guo, Q.; Liu, L. Removal of formaldehyde at low concentration using various activated carbon fibers. *J. Appl. Polym. Sci.* **2007**, *106*, 2151−2157.

(38) Vishnyakov, A.; Ravikovitch, P. I.; Neimark, A. V.; Bülow, M.; Wang, Q. M. Nanopore Structure and Sorption Properties of Cu−BTC Metal−Organic Framework. *Nano Lett.* **2003**, *3*, 713−718.

(39) Sánchez-González, E.; Mileo, P. G. M.; Sagastuy-Breña, M.; Álvarez, J. R.; Reynolds, J. E.; Villarreal, A.; Gutiérrez-Alejandre, A.; Ramírez, J.; Balmaseda, J.; González-Zamora, E.; Maurin, G.; Humphrey, S. M.; Ibarra, I. A. Highly reversible sorption of H_2S and CO_2 by an environmentally friendly Mg-based MOF. *J. Mater. Chem. A* **2018**, *6*, 16900−16909.

(40) Gao, P.; Sun, X.-Y.; Liu, B.; Lian, H.-T.; Liu, X.-Q.; Shen, J.-S. Cu MOF-based catalytic sensing for formaldehyde. *J. Mater. Chem. C* **2018**, *6*, 8105−8114.

(41) Vikrant, K.; Qu, Y.; Szulejko, J. E.; Kumar, V.; Vellingiri, K.; Boukhvalov, D. W.; Kim, T.; Kim, K.-H. Utilization of metal−organic frameworks for the adsorptive removal of an aliphatic aldehyde mixture in the gas phase. *Nanoscale* **2020**, *12*, 8330−8343.